Rainbowlike effects in (^{3}He,α) reactions

V. Burjan, J. Cejpek, J. Fojtů, V. Kroha, and I. Pecina
Nuclear Physics Institute, Academy of Sciences of Czech Republic, 250 68 Řež, Czech Republic

A. M. Mukhamedzhanov and N. K. Timofejuk
Nuclear Physics Institute, Uzbek Academy of Sciences, 702 132 Tashkent, Uzbekistan
(Received 24 July 1992; revised manuscript received 6 April 1993)

The angular distributions of the elastic scattering and (^{3}He,α) cross sections for 37.9 MeV ^{3}He particles incident on target nuclei ^{13}C and ^{14}C were analyzed from the standpoint of possible presence of the refractive effects in one-nucleon transfer reactions. The analysis of experimental data is given in the framework of the distorted wave Born approximation using external microscopically calculated form factors. The presence of the rainbowlike mechanism in both elastic and reaction channels was observed. The effect is apparent mainly for transitions where strong orbital mismatching occurs.

PACS number(s): 24.50.+g, 25.55.Hp

I. INTRODUCTION

It is well known that in the elastic scattering of ^{3}He and α particles on 1p-shell nuclei (for $A > 10$ and incident energies of tens MeV/nucleon) rainbow effects are observed [1,2]. These effects clearly manifest optical properties of the quantum scattering of light ions and allow one to get information about the nuclear optical potential in the nuclear interior. The same effect was found in charge-exchange reactions (^{3}He,t) [2] which can also be considered (in the isospin formalism) as elastic scattering.

Let us briefly outline characteristic features of the "rainbowlike" mechanism: (1) In the angular distributions of elastic scattering the domain of the Frauenhofer interference is followed by a broad bump with an exponential descent towards large angles. This behavior is described by the Airy function [3]. (2) The form of the angular distribution about the main maximum does not depend on the imaginary part of the optical potential—only its absolute value changes. (3) This whole domain is determined essentially by the far-side component of the reaction amplitude. For the rainbowlike mechanism, a partial transparency of the nucleus is necessary also for smaller orbital momenta than values corresponding to the surface domain $l \approx kR_s$ [where k is given by the energy of the particle in the corresponding reaction channel and R_s is the strong absorption radius defined as $R_s \approx 1.5 (A_1^{1/3} + A_2^{1/3})$].

It has been shown that for reactions with good matching of the initial and final angular orbital momentum the main contribution to the reaction amplitude comes from the external surface region of the nucleus-target interaction [4]. The contribution from the nuclear interior can be usually neglected because of the strong volume absorption for such incident energies.

The extent of refractive effects in the case of severely mismatched reactions such as (^{3}He,α), when the contribution of the nuclear interior cannot be neglected [4], is not fully understood. In this case one can hope that if rainbow scattering is seen in elastic scattering then it could be observed in the nuclear reaction, too. This expectation is based on the following qualitative consideration: If there exists a rainbowlike elastic scattering mechanism in the entrance channel ^{3}He+C, it gives evidence, in the classical interpretation, for an amplification of the contribution of some trajectories (caustic) corresponding to a certain interval of reaction angles. It also indicates that there is some transparency for lower partial waves as there occurs a typical interference characterized by an Airy function. If it is so in the ^{3}H+C channel, and if we know that there exists a nonnegligible influence of an inner domain of the nucleus onto the (^{3}He,α) reaction amplitude (because of strong momentum mismatching) [4], then it is interesting to investigate if these circumstances manifest themselves in the mechanism of this reaction, too.

The aim of this work was to test this idea by measuring the differential cross sections of the (^{3}He,α) reaction on the ^{13}C and ^{14}C targets at energies $E \approx 38$ MeV (in the laboratory system). At the same time we measured the angular distributions of the elastic scattering of ^{3}He on both nuclei. The rainbow effect was observed both in elastic scattering and transfer reactions.

The rainbow effects in the (^{3}He,α) reactions in such an energy region could be seen for the first time in our preliminary communication [5] for ^{13}C(^{3}He,α) ^{12}C(g.s) only. A study [6] performed recently at the energies 50 and 60 MeV seems to confirm our conclusions. In Ref. [2] an attempt to interpret the results of the paper [7] in terms of rainbow scattering is mentioned which, however, was not made in the original paper. The first observation of the rainbow effects in a one-neutron transfer was in a heavy ion reaction ^{12}C(^{13}C,^{12}C)^{13}C [8], but it seems that further analysis for this case is needed. Some features similar to those observed by us might be identified in the reaction ^{17}O(^{3}He,α)^{16}O [9], namely some traces of rainbow for the ground state transition which disappear as one goes to the highly excited states with better momentum matching. This previous work was a part of a series of studies made for several light targets from ^{9}Be up to ^{54}Fe, see e.g.

[10], [11], and [12], but in all these cases nobody has looked for rainbow effects.

For analysis of reactions with a large Q value it is very important to have reliable form factors (overlap integrals) to determine the reaction amplitude. Therefore a detailed discussion of the calculation of these quantities is presented in this work.

In Sec. II the experimental method is briefly described. An overview of the analysis, techniques, and theoretical methods to calculate the overlap integrals are given in Sec. III. In Sec. IV the experimental results and their analysis are presented.

II. EXPERIMENTAL METHOD

The experiments were performed on the ^{3}He beam with the energy 37.9 MeV using the isochronous cyclotron U-120M of the Nuclear Physics Institute of Academy of Sciences of Czech Republic at Řež. The angular distribution measurements were carried out by means of four E-ΔE telescopes placed in a target chamber. Both ΔE and E silicon detectors were the surface-barrier type of thicknesses 150 and 2000 μm, respectively. These detectors were cooled to -35 °C. The on-line mass identification of reaction products was accomplished using a special fast digital peripheral processor. Errors in the angular measurements were reduced by stabilizing the beam position on the target. This stabilization was achieved with a correcting feedback system which consisted of microchannel detectors inside a diagnostic chamber. These detectors allowed the visualization of the beam trace on a screen. The picture of this trace from a TV camera was digitized and mathematically processed by a computer which then provided the error signal for the correcting magnet. Details of this method are briefly described in Ref. [13]. The average error of the reaction angle was kept to about 0.1°.

The thickness of the self-supporting targets was carefully measured by the shift method using the change in energy of collimated α particles of the ^{228}Th nuclide after transition through targets. The central area of each target was systematically scanned and the thicknesses were found to be 0.165 mg/cm^2 for ^{13}C and 0.180 mg/cm^2 for ^{14}C. The average errors of measurements did not exceed 5%. The ^{13}C and ^{14}C targets were enriched to 76.4% and 80%, respectively.

The evaluated average error of absolute differential cross sections which included uncertainties due to the target thickness, charge measurement, solid angle determination, dead time counting, statistical errors, etc. was of the order of 5% for laboratory angles up to $\sim 50°$ and less than 10% for other angles.

III. OVERLAP INTEGRALS AND VERTEX FORM FACTORS

The distorted wave Born approximation (DWBA) amplitude of the nuclear transfer reaction $A(a,b)B$, where $A=B+n$, $b=a+n$, and n is a transferred neutron, is given by the expression

$$M^{DW}=\langle \Psi_f^{(-)}|F_{fi}|\Psi_i^{(+)}\rangle \ . \tag{1}$$

The $\Psi_i^{(+)}$ and $\Psi_f^{(-)}$ are the distorted waves in the entrance and exit channels, respectively; F_{fi} is the form factor

$$F_{fi}=\langle Bb|V_{an}|An\rangle=\langle \Psi_{J_BM_B}\Psi_{J_bM_b}|V_{an}|\Psi_{J_AM_A}\Psi_{J_aM_a}\rangle$$

$$=\sum_{\substack{ll'jj'\\ m_lm_{l'}\\ m_jm_{j'}}}(jm_jJ_BM_B|J_AM_A)(lm_l\tfrac{1}{2}\sigma|jm_j)(j'm'_jJ_aM_a|J_bM_b)$$

$$\times(l'm'_l\tfrac{1}{2}\sigma|j'm'_j)I_{ABn}(l_{j'}r_{Bn})\Phi_{ban}(l',j',r_{an})Y_{lm_l}(\hat{\mathbf{r}}_{Bn})Y^*_{l'm_l}(\hat{\mathbf{r}}_{an}) \ , \tag{2}$$

where V_{an} is the interaction potential of particles a and n, $\mathbf{r}_{ij}=\mathbf{r}_i-\mathbf{r}_j$, $\mathbf{r}_i$ being the radius vector of the center of mass of a particle i, $\hat{\mathbf{r}}=\mathbf{r}/r$; I_{ABn} and Φ_{ban} stand for the radial parts of the overlap integral $\langle \Psi_{J_BM_B}|\Psi_{J_AM_A}\rangle$ and the "potential overlap" integral $\langle \Psi_{J_bM_b}|V_{an}|\Psi_{J_aM_a}\rangle$ respectively, $\Psi_{J_iM_i}$ is the internal wave function of the nucleus i with the spin J_i and its projection M_i. The integration is performed over all coordinates of the nucleons of nuclei B and a, respectively.

The calculation of these quantities is the crucial point in the theory of transfer reactions. The well-known approximation in the standard DWBA is used (for brevity we omit quantum numbers l,j in overlap integrals):

$$I_{XYn}(r)=S^{1/2}\varphi(r) \tag{3}$$

where $\varphi(r)$ is the radial single-particle wave function of the nucleon bound state in a nucleus X calculated in the Woods-Saxon potential and S is the spectroscopic factor of that state. To find the parameters of such potential the well-depth procedure is usually used. However, in such an approach the significant dependence of the overlap integrals on the geometrical parameters of the Woods-Saxon potential is hidden. The many particle character of the problem is ignored and the Pauli principle is not taken properly into account. Additionally, there is a principal shortcoming of such a procedure: the overlap integral is calculated up to the normalizing constant only, which then calibrates the absolute value of the differential cross section. Usually, a search for this constant is the main task of the DWBA analysis of experimental data. The reliability of such spectroscopic factors depends on

the correctness of the approximation used in the derivation of Eq. (3) which may be, however, quite dubious in the nuclear interior.

In the external region which gives the dominant contribution to the cross section at small angles the overlap integral can be approximated by its asymptotic behavior:

$$I_{XYn}(r)\sim C_{XYn}\exp(-\kappa_{Yn}r)/r\ ,\quad r\to\infty \tag{4}$$

where $\kappa_{Yn}^2=2\mu_{Yn}\varepsilon_{Yn}$, ε_{Yn} is the binding energy of particles Y and n in the bound state (Yn), $\mu_{Yn}=m_Y m_n/(m_Y+m_n)$ and C_{XYn} is the asymptotic normalization coefficient (ANC) which is proportional to the vertex constant (VC) G_{XYn} for the neutron removal from the nucleus [14]

$$|G_{XYn}|^2=\pi(\hbar/\mu_{Yn}c)^2C_{XYn}^2\ . \tag{5}$$

G_{XYn} defines the normalization of the external region contribution to the reaction amplitude. This quantity, which is the fundamental nuclear characteristics, can be extracted, in principle, in a model independent way. For example, it could be deduced from sub-Coulomb nucleon transfer reactions when the contribution from the nuclear interior is negligible and the cross section is proportional to $|G_{XYn}|^2$ only, from heavy-ion reactions at low energies when the absorption is strong enough or by extrapolation of the differential cross sections to the nearest singularity point in the complex $\cos\vartheta$ plane (ϑ is the reaction angle in the c.m. system) [15]. The problem of calculation of the overlap integrals in the nuclear interior has not yet been solved.

In our DWBA analysis we used the microscopic method. The idea of the method is based on the connection between $I_{XYn}(q)$ and the vertex form factors $G_{XYn}(q)$ appearing in the dispersion theory of nuclear reactions [14,16]:

$$I_{XYn}(q)=-4\mu_{Yn}\left[\frac{\pi}{N_x}\right]^{1/2}G_{XYn}(q)/(q^2+\kappa_{Yn}^2)\ , \tag{6}$$

$$I_{XYn}(r)=-\frac{^2\mu_{Yn}}{\pi^{3/2}N_x^{1/2}}\times\int_0^\infty dq\,q^2 j_1(qr)G_{XYn}(q)/(q^2+\kappa_{Yn}^2)\ , \tag{7}$$

N_x resulting from the identity of nucleons is equal to the atomic number of nucleus X according to isospin formalism. To determine $I_{XYn}(r)$ or $I_{XYn}(q)$ it is sufficient to calculate the vertex form factor $G_{XYn}(q)$ which is defined by the expression [14]

$$G_{XYn}(q)=(4\pi N_x)^{1/2}\sum_{m_l m_j M_y}(jm_jJ_yM_y|J_xM_x)(lm_l\tfrac{1}{2}\sigma|jm_j)\chi^+_{(1/2)\sigma}\chi^+_{(1/2)\tau}\int d\mathbf{r}\,j_l(qr)Y^*_{lm_l}\left[\frac{\mathbf{r}}{r}\right]\langle\Psi_{J_yM_y}|V_{Yn}|\Psi_{J_xM_x}\rangle\ . \tag{8}$$

Here $\chi^+_{(1/2)\sigma}$ and $\chi^+_{(1/2)\tau}$ are the spin and isospin nucleon wave functions. It is worth noting that the on-shell value of $G_{XYn}(q=i\kappa_{Yn})$ is the vertex constant mentioned above, $G_{XYn}(i\kappa_N)=G_{XYn}$. To calculate $G_{XYn}(q)$ we should select the wave functions of nuclei X and Y. In this work we used the wave functions of the translationally invariant oscillator shell (TISM) model, which is the most suitable from the practical standpoint. The main shortcoming of these functions is an incorrect asymptotic behavior. For this reason they are usually not used for the calculation of cross sections of transfer reactions, which are thought to occur at the nuclear surface. Nevertheless, using Eq. (8) we can obtain the overlap integrals $I_{XYn}(r)$ with a correct radial dependence for $r\to\infty$ even in such a case [16]. This assumption follows from the presence of the nuclear potential V_{Yn} in Eq. (8) which damps the contribution to the integral over r' in the outer region where the oscillator wave functions would not be suitable. The correct asymptotic dependence of $I_{XYn}(r)$ is provided by the existence of a pole at $q^2=-\kappa^2$ in the integrand of Eq. (7) [14].

Let us consider the potential V_{Yn}. It is the sum of NN potentials and in the self-consistent problem it is necessary to take into account such potentials to calculate internal wave functions of nuclei X and Y. In this work we used TISM wave functions of Boyarkina [17] which are not the solutions of the Schrödinger equation with a certain NN potential. However, the proper choice of such a potential is of great importance because, as follows from calculations [16], different NN potentials give different values of G_{XYn}. In our work we used the potential M3YE [18] containing central, spin-orbit and tensor parts optimized according to matrix elements of Elliot [19]. Therefore, such a potential is closely related to self-consistency. This potential was reported to be the best of all the tested ones in describing all reliably established VCs for the $1p$-shell nuclei [16]. Similar values of VC, $|G_{^{13}C^{12}C_n}|^2=0.39\pm0.02$ fm were obtained for example, for the virtual decay $^{13}C\to{}^{12}C(g.s.)+n$ from various experiments. We obtained from Eq. (8) with the potential M3YE, for $q=i\kappa_{Yn}$, the value $|G_{^{13}C^{12}C_n}|^2=0.41$ fm. A reliable value of this quantity for the vertex $\alpha\to{}^3He+n$ is not known. The range of various estimates is between 5.7 to 17.6 fm. Present calculations of VC by the solution of Yakubovsky equation with the NN potential from the composed quark bag model gave the value $|G_{\alpha^3Hen}|^2=5.7$ fm [20]. Our calculation with the M3YE potential gives $|G_{\alpha^3Hen}|^2=6.9$ fm, which is in reasonable agreement with the preceding value. Therefore in our DWBA analysis described below, the same potential M3YE was used for calculation of both overlap integrals.

In summary, in the DWBA analysis of experimental data the overlap integrals containing both light and heavy vertex in the form factor of the reaction amplitude were calculated microscopically according to Eqs. (5) and (7). The wave function of TISM and the NN potential M3YE were used. Such an approach is free of any fitting

parameters, like the geometrical ones of a Woods-Saxon potential and spectroscopic factors which calibrate the absolute value of differential cross sections. Use of microscopic form factors allows us, to some extent, to take into account the many particle effects as well as the effects of antisymmetrization. The correct asymptotic normalization of overlap integrals ensures an accurate determination of the contribution of the external region to the reaction amplitude. In our approach, the only "free" parameters in DWBA are those associated with uncertainties of the optical parameters in the entrance and exit channels.

IV. ANALYSIS OF THE EXPERIMENTAL DATA

Angular distributions from 8° to 160° (lab) for the differential cross section of the elastic scattering and (^{3}He,α) reaction on ^{13}C and ^{14}C were measured using a 37.9 MeV ^{3}He beam. In the reaction channel, data were extracted for the 0.00, 4.44, 7.66, and 15.11 MeV states in ^{12}C and 0.00, 3.68, and 15.11 MeV states in ^{13}C. Analysis of the elastic scattering data was performed using the code ECIS 79 [22] while DWUCK 5 [21], modified to allow the use of the external form factors, was employed in the (^{3}He,α) studies.

A. The reaction ^{13}C(^{3}He,α)^{12}C(g.s.)

In Fig. 1(a) the angular distribution of the scattering is shown. The distribution is characterized by the rainbow-like behavior: oscillations at small angles and deep minimum followed by a wide peak which decreases gradually towards large angles. Different optical potential sets were tested to describe elastic cross section. It was found that there exist several potentials which give almost equally good descriptions of the cross section in the entire angular region. However, all of these potentials had to incorporate both volume and surface absorption terms, indicating a more complicated radial dependence. Potentials without such a combination are not able to describe the angular distribution; in particular the "rainbow" region of angles is poorly reproduced. Similar results were obtained in Ref. [2]. A sample of two such potentials are given in Table I as set A1 from Ref. [2] and A2 from the present work. The best results were obtained with the potential A2 which corresponds to the optimal fit of the experimental data. The spin-orbit part was neglected as unimportant in the effect on the differential cross section. This A2 potential gives the best description of the reaction cross section, as seen in Fig. 2(a). The corresponding near side–far side decomposition of the scattering cross section as well as the angular distribution (multiplied by factor $\frac{1}{10}$) for no absorption ($W=0$) is also shown in this figure. This calculation confirms the presence of the refractive mechanism in the elastic scattering at $E\sim 38$ MeV. From Fig. 2(a) it is evident that the angular distribution of the analyzed reaction has the typical characteristics of such a mechanism and the rainbow peak approximately coincides with the wide maximum in the scattering channel.

As mentioned previously, microscopically calculated overlap integrals with the correct asymptotic behavior were used in the analysis of the experimental data in a DWBA framework. Both integrals $I(\alpha^3\mathrm{He}n)$ and $I(^{13}\mathrm{C}^{12}\mathrm{C}n)$ were calculated with the same M3YE potential. In Fig. 3 the radial dependence of "heavy" overlap integrals is presented. As noted in the previous part, there are no free parameters connected with the structure of nuclei in this approach. The quality of the agreement between experimental data and the theory depends on the adequacy of the DWBA and on a proper choice of the optical potentials. Unfortunately, we did not have experimental data for the elastic α scattering in the relevant energy region. Therefore, we used several different potentials which covered both deep and shallow real central potentials from the literature, some of which are given in Table I as B1–B4. The potentials listed describe the experimental α scattering by the ^{12}C nucleus for alpha energies of 56 MeV (B1–B3) and 65 MeV (B4) [26]. The α-particle elastic scattering angular distribution does not exhibit an unambiguous rainbowlike feature at these energies, but its presence cannot be excluded. In Fig. 2(b)

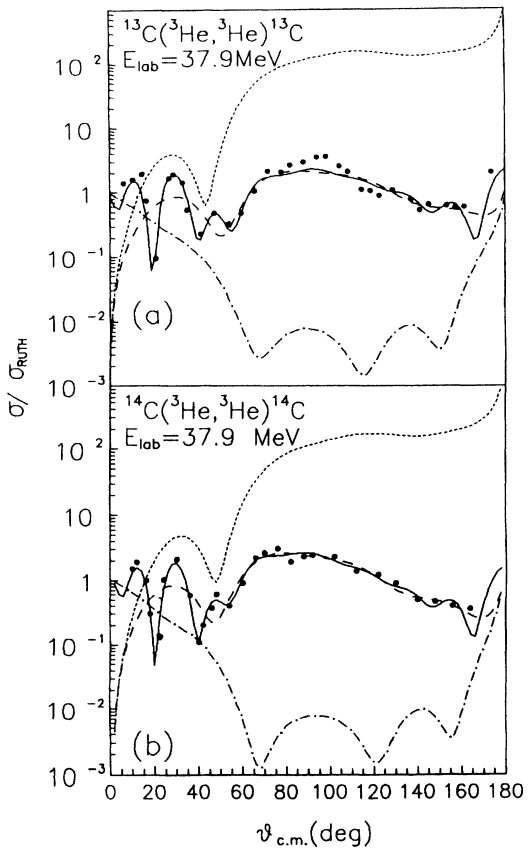

FIG. 1. (a) Differential cross-section angular distribution for the elastic scattering of 37.9 MeV ^{3}He particles on ^{13}C. Full circles: experimental points; solid line: full cross section; dashed line: far-side component; dash-dotted line: near-side component; dotted line: calculated far-side component without absorption. All the curves were obtained with the potential A2. (b) Same as (a) for ^{14}C. Theoretical curves were calculated with the potential C1 (see Table I).

the DWBA calculations with different combinations of optical parameters are given. It is seen that the calculated angular distributions are strongly dependent on α-particle optical model parameters especially when comparing the "rainbow" angular region ($\vartheta_{c.m.} \sim 40-100°$). The region of this sensitivity corresponds to nuclear distances about 3 fm. The radius of the strong absorption is in this case $R_s \sim 5$ fm.

The best description of experimental angular distributions was achieved by the A2–B2 potential combination. The shallow potentials in the output channel (B1 and B4 as the example) do not describe experimental data in the "rainbow" region. In Fig. 2(b) the theoretical cross section with the standard form factor (by the "well-depth" procedure) is also given. The corresponding curve has to be normalized to the experimental points (by the usual spectroscopic factor). Nevertheless, its shape does not seriously differ from a microscopic one. This similarity

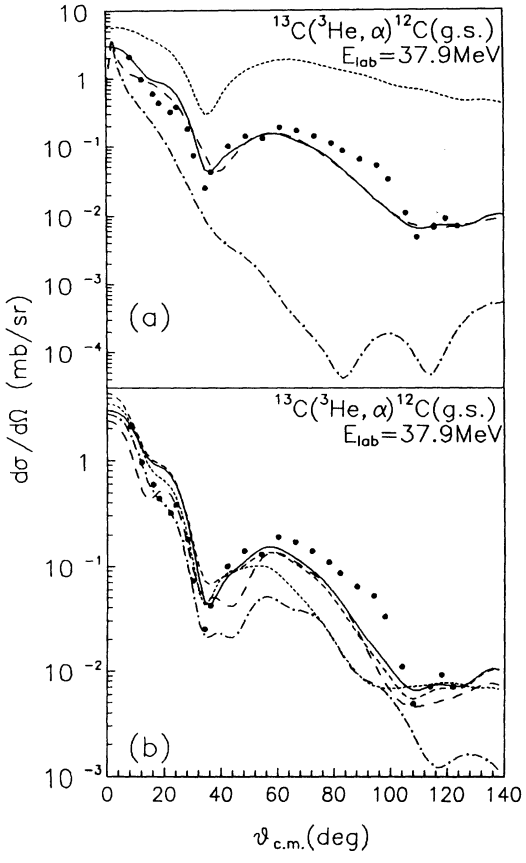

FIG. 2. (a) Differential cross section angular distribution for the ^{13}C(^{3}He,α)^{12}C(g.s.) reaction. Full, dashed, and dash-dotted lines are the full, far-side, and near-side components of the reaction cross section, respectively. Calculated curves correspond to the potentials A2-B2; see Table I. The dotted line represents calculation with $W=0$ in the entrance channel. (b) Calculations showing the effect of using the different optical model parameters for both entrance and exit channels (see Table I): full line: potentials A2-B2; dashed line: potentials A1-B2; dash-dotted line: potentials A2-B4; dotted line: potentials A2-B3; short dashed line: potentials A2-B2 with the standard "well-depth" form factor. This curve is normalized to experimental points.

TABLE I. Optical model parameters used in the analysis of the (^{3}He,α) reactions.

Target	Channel	Label	$-V$ (MeV)	r_V (fm)	a_V (fm)	$-W$ (MeV)	r_W (fm)	a_W (fm)	V_D (MeV)	r_D (fm)	a_D (fm)	V_{SO} (MeV)	r_{SO} (fm)	a_{SO} (fm)	$\frac{J_V}{3A}$	
^{13}C	^{3}He	A1	151.6	0.84	0.833	4.90	2.28	0.487	5.88	1.46	0.600	5.43	1.37	0.475	351	a
		A2	103.0	1.19	0.811	2.39	1.33	0.572	10.71	1.19	0.876				444	b
	α	B1	115.5	1.50	0.555	24.00	1.5	0.400								c
		B2	151.9	1.24	0.665	28.05	1.24	0.640								c
		B3	216.8	1.30	0.580	28.05	1.50	0.320								c
		B4	120.7	1.28	0.767	9.133	2.10	0.363	31.81	0.966	0.24					d
^{14}C	^{3}He	C1	96.23	1.202	0.821	1.88	1.665	0.614	9.34	1.216	0.878				419	b
		C2	124.0	0.94	0.826	2.10	2.66	0.483	20.9	1.12	0.342	2.71	1.19	0.580	335	a

[a]Parameters from Ref. [2].
[b]Present work, best fit.
[c]Parameters from Ref. [23].
[d]Parameters corresponding to experimental data of Ref. [26].
In all cases the Coulomb radius $r_c = 1.30$ fm was used.

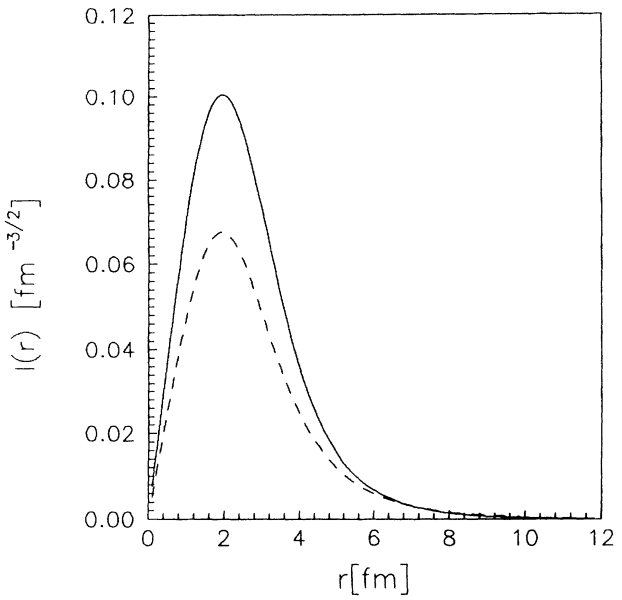

FIG. 3. Radial part of the nuclear overlap integrals. The full line is $I(^{14}C^{13}Cn)$ while the dashed line corresponds to $I(^{13}C^{12}Cn)$.

indicates that the main contribution to the amplitude of this reaction comes from the outer region where the asymptotic behavior of both form factors are similar.

In Fig. 2(a) the calculated reaction differential cross section without the absorption in the input channel is also given. It is seen, as in the case of the elastic scattering [see Fig. 1(a)], that the overall behavior of the angular distribution is qualitatively well described, showing similarity of both mechanisms. Therefore, one can say that the presence of the nuclear rainbow in the reaction channel is probably driven by the rainbow mechanism in the entrance scattering channel.

It is worthwhile to calculate the corresponding spectroscopic factor. In terms of microscopic overlap

$$S=\langle I_{XYn}|I_{XYn}\rangle\ , \tag{9}$$

where I_{XYn} is the radial overlap integral in question. The factor following from the identity of nucleons is included in I_{XYn}. According to (9) we obtained a spectroscopic factor for the single-particle state $^{12}C(g.s.)+n$ in $^{13}C(g.s.)$ as $S=0.74$ which is close to the theoretical value $S=0.67$ calculated in TISM using the wave functions of Boyarkina [17]. For comparison, the value of Cohen and Kurath's calculation is $S=0.61$ [24]. The spectroscopic factor extracted by the usual well-depth procedure [see Fig. 2(b)] is $S=0.45\pm0.05$. The spectroscopic factor for the ^3He+n state in the α particle given by (9) is $S=1.3$ while TISM gives $S=2$.

B. The reaction $^{13}C(^3He,\alpha)^{12}C^*$

In Fig. 4(a) the experimental cross sections for different excited states of ^{12}C are given. It is shown that in the case of the 2^+, 4.44 MeV ($Q=11.2$ MeV) state the angular distribution has the characteristic "rainbow" decline starting from $\vartheta_{c.m.}\sim60°$ but without the typical deep minimum at smaller angles. In other words, the effect of this mechanism, if present, is not so strong as for the ground state transition. For other excited states—0^+, 7.66 MeV ($Q=7.97$ MeV) and the analog state 1^+, 15.11 MeV ($Q=0.52$ MeV)—the effect of the rainbowlike mechanism disappears.

Unfortunately, reliable microscopically calculated overlap integrals for excited states of ^{12}C are not available. Therefore, the theoretical curves in Fig. 4 are calculated by the standard well-depth procedure and normalized to the experimental points. Corresponding spectroscopic factors obtained in this way are $S(2^+)=0.41\pm0.04$, $S(0^+)=0.031\pm0.01$, and $S(1^+)=2.6\pm0.3$. The best combination of the optical potentials corresponds to the set 2A–B2 for all states. It is well known that detailed comparison of the experimental and theoretical differential cross sections for the case of $(^3He,\alpha)$ reactions on light nuclei is difficult without properly calculated form factors. Similarly, interpretation of the standard spectroscopic factors is questionable espe-

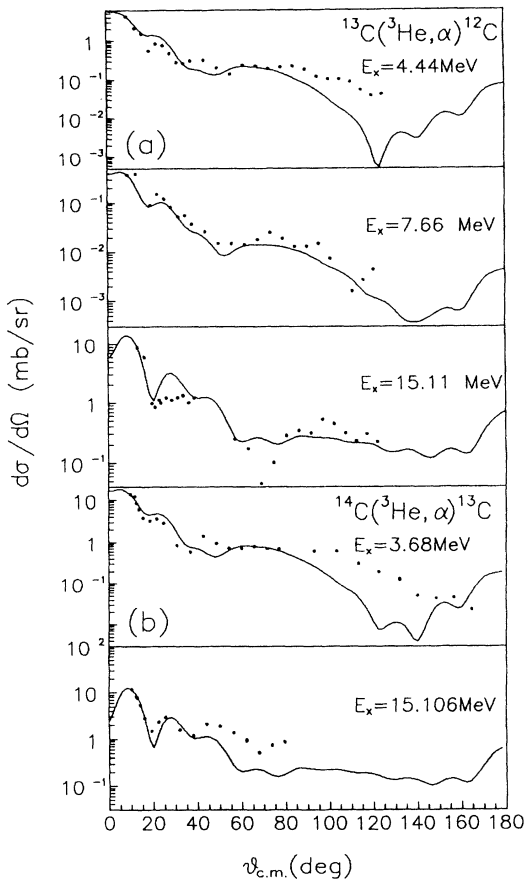

FIG. 4. Experimental differential cross section angular distribution for excited states, (a) in the $^{13}C(^3He,\alpha)$ ^{12}C reaction, (b) in the $^{14}C(^3He,\alpha)$ ^{13}C reaction. The curves for all transitions correspond to standard DWBA calculations using a well-depth procedure and the optical potential sets A2-B2 for the first and C1-B2 for the second reaction.

cially for analog states. The generalization of existing methods of the form factor calculations will be a subject of further investigations.

Nevertheless, we can make the qualitative conclusion that the rainbow mechanism is observed in (^{3}He,α) transfer reactions, where a strong angular momentum mismatching is present. For higher excitations (with better matching) this mechanism is not so important and for the best matching of the orbits ($Q \sim 0$) we can observe the diffraction typical for the strong absorption mechanism.

C. The reaction ^{14}C(^{3}He,α)^{13}C(g.s.)

The differential cross section angular distribution for the elastic scattering of ^{3}He on the ^{14}C nucleus is presented in Fig. 1(b) and the (^{3}He,α) reaction differential cross section in Fig. 5(a). The ^{3}He optical parameters used are given in Table I as C1 and C2. The best fit of the elastic scattering corresponds to parameters C1. As in the previous case of the scattering on the ^{13}C nucleus we can see the typical rainbowlike behavior with a characteristic Airy maximum. Since in the literature there are no available data for α scattering on the ^{13}C in our energy region, we used the same optical model parameters as for the ^{13}C(^{3}He,α)^{12}C reaction, see Table I. The microscopically calculated form factors were also used both for the "light" and for the "heavy" vertices. Note that our M3YE potential gives a value of the vertex constant $|G(^{14}\mathrm{C}^{13}\mathrm{C}n)|^2 = 3.18$ and $S = 1.69$. The spectroscopic factor deduced by means of the standard well-depth procedure [see Fig. 5(b)] is 1.1 ± 0.1. Theoretical values of S are 1.76 from TISM [17] and 1.73 from Cohen and Kurath [24].

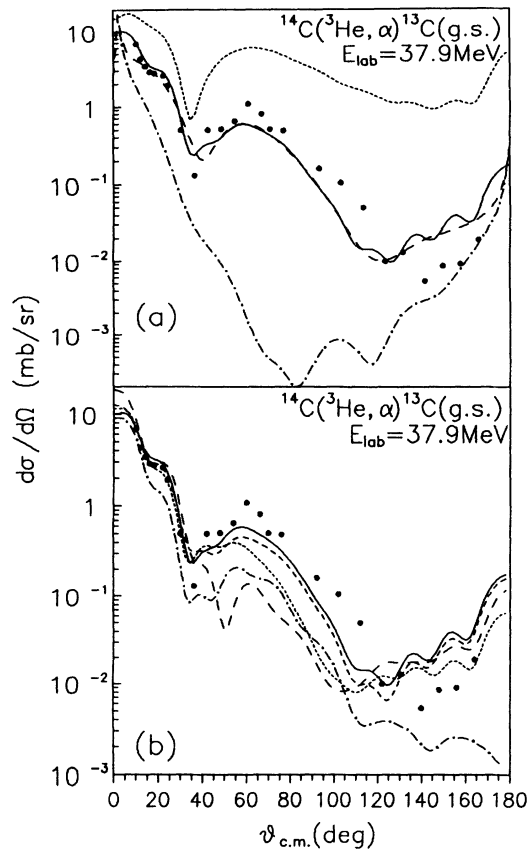

FIG. 5. Differential cross section angular distribution for the ^{14}C(^{3}He,α)^{13}C(g.s.) reaction. (a) Same as Fig. 2(a), calculated curves correspond to the optimum set of optical potentials C1-B2 (see Table I). The dotted line is the calculation with $W=0$ for the entrance channel. (b) Same as Fig. 2(b), full line: potentials C1-B2; dashed line: potentials C1-B3; dash-dotted line: potentials C2-B4; dotted line: potentials C2-B2; short dashed line: potentials C1-B2 with the standard "well-depth" form factor. The normalization is as in Fig. 2(b).

The best description of the angular distribution was obtained with potential parameters C1–B2. The calculated differential cross section is in reasonable agreement with the experiment both qualitatively and in the absolute value. As in the case of the ^{13}C target, the only free parameters in calculations were the optical potential ones. Differences between exit channel optical-model parameter sets are manifested mainly in the "rainbow" region of angles while in the vicinity of the main maximum they give practically the same results. These differences are demonstrated in Fig. 5(b). In this figure the effect of the form factor is presented with the same normalization of the "well-depth" curve as is shown in Fig. 2(b).

D. The reaction ^{14}C(^{3}He,α)^{13}C*

The measured angular distributions for excited states of ^{13}C—$\frac{3}{2}^-$, 3.68 MeV ($Q = 8.72$ MeV)—and the analog state $\frac{3}{2}^-$, 15.11 MeV ($Q = -2.70$ MeV) are given in Fig. 4(b). Again we see that rainbowlike effects for excited states in these reactions gradually disappear and for the 15.11 MeV state transition the angular distribution exhibits the diffraction pattern. For the same reasons as in the Sec. IV B the theoretical differential cross section has been calculated in a standard DWBA framework. The optical potentials used correspond to sets C1-B2. Corresponding spectroscopic factors are $S(\frac{3}{2}^-) = 1.3 \pm 0.1$ for the 3.68 MeV state and $S(\frac{3}{2}^-) = 4.0 \pm 0.4$ for the 15.106 MeV analog state.

V. CONCLUSIONS

The differential cross section of the (^{3}He,α) reactions on the ^{13}C and ^{14}C nuclei as well as the elastic scattering in entrance channels were measured for the incident ^{13}He of energy $E = 37.9$ MeV.

For the case of the ground-state transition with the maximum momentum mismatching the possible presence of the rainbowlike mechanism was established. A similar mechanism manifests itself in the entrance elastic channels.

A theoretical analysis of reaction channel angular distributions for ground-state transitions was carried out in the framework of DWBA with a microscopically calculated form factor. An adequate quantitative description was obtained without any free structural parameters.

It was shown that the optical potentials which optimally describe the rainbow mechanism of the elastic scattering could be further selected according to the shape of the reaction differential cross section. Therefore, although the well-known ambiguity of the optical-model potentials is not eliminated, it may be essentially reduced.

The mechanism of both transfer reactions was analyzed using a coupled-channel basis (using the program CHUCK [25]). It was found that the coupling with inelastic channels is negligible.

It was also found that the rainbowlike mechanism of transfer reactions seems to occur for the case of strong orbital momentum mismatching only. Decreasing the Q value leads to a gradual reduction of this effect. We can therefore assume that for smaller Q (better matching) the transfer reaction is more quasielastic, i.e., more peripheral in an output channel and the mechanism is more diffractive. This effect will, however, be dependent on energy of the incident particles. It is, of course, only a qualitative conclusion. More extensive experimental and theoretical study of the refractive processes in transfer reactions would be very desirable because they can give valuable information about the interactions at small distances in the region of the nuclear form factors.

[1] D. A. Goldberg, S. M. Smith, and G. F. Burdzik, Phys. Rev. C **10**, 1362 (1974).
[2] A. S. Dem'yanova *et al.*, Phys. Scr. **T32**, 89 (1990).
[3] K. W. Ford and J. A. Wheeler, Ann. Phys. (N.Y.) 7, 259 (1959).
[4] I. R. Gulamov *et al.*, Czech. J. Phys. **B40**, 875 (1990).
[5] A. M. Mukhamedzhanov *et al.*, Yad. Fiz. **52**, 704 (1990) [Sov. J. Nucl. Phys. **52**, 452 (1990)].
[6] V. V. Adodin *et al.*, Yad. Fiz. **55**, 577 (1992) [Sov. J. Nucl. Phys. **55**, 319 (1992)].
[7] T. Tanabe *et al.*, J. Phys. Soc. Jpn. **41**, 361 (1976).
[8] H. G. Bohlen *et al.*, Z. Phys. A **322**, 241 (1985).
[9] O. Karban *et al.*, Phys. Lett. **112B**, 433 (1982).
[10] N. M. Clarke *et al.*, J. Phys. G **5**, 1233 (1979).
[11] R. J. Griffiths *et al.*, J. Phys. G. **7**, 381 (1981).
[12] P. M. Lewis *et al.*, Nucl. Phys. **A395**, 204 (1983).
[13] V. Bejsovec *et al.*, in *Proceedings of International Cyclotron Conference, Bechyne, Czechoslovakia, 1985,* edited by D. L. Novikov (Joint Institute of Nuclear Research, Dubna, 1986), p. 235.
[14] L. D. Blokhincev, I. Borbely, and E. I. Dolinski, Phys. Elem. Part. At. Nucl. **8**, 1189 (1977).
[15] I. Borbely, J. Phys. G **5**, 937 (1979).
[16] A. M. Mukhamedzhanov and N. K. Timofejuk, Yad. Fiz. **51**, 679 (1990) [Sov. J. Nucl. Phys. **51**, 431 (1990)].
[17] A. N. Boyarkina, *Structure of 1 -p Shell Nuclei* (Moscow State University Press, Moscow, 1973).
[18] G. Bertsch *et al.*, Nucl. Phys. **A284**, 399 (1977).
[19] J. P. Elliot *et al.*, Nucl. Phys. **A121**, 241 (1968).
[20] A. G. Barishnikov *et al.*, Yad. Fiz. **48**, 1273 (1988) [Sov. J. Nucl. Phys. **48**, 809 (1988)].
[21] P. D. Kunz, code DWUCK 5 (unpublished).
[22] J. Raynal, code ECIS 79 (unpublished).
[23] P. Gaillard *et al.*, Nucl. Phys. **A131**, 353 (1969).
[24] S. Cohen and D. Kurath, Nucl. Phys. **A101**, 1 (1967).
[25] P. D. Kunz, code CHUCK (unpublished).
[26] M. Yasue *et al.*, Nucl. Phys. **A394**, 29 (1983).